MINISTRY OF EDUCATION AND TRAINING

VIETNAM ACADEMY OF SCIENCE AND TECHNOLOGY

GRADUATE UNIVERSITY OF SCIENCE AND TECHNOLOGY

NGO THI LAN

RESEARCH ON THE PHYSICAL INTERACTION BETWEEN DELOCALIZED AND LOCALIZED ELETRONS IN Au_9M^{2+} (M = Sc-Ni) AND Ag_nCr (n = 2-12) ALLOY NANOCLUSTERS SYSTEMS USING DENSITY FUNCTIONAL THEORY

SUMMARY OF DISSERTATION ON ELECTRONIC MATERIAL

Code: 9.44.01.23

Ha Noi – 2024

The dissertation is completed at: Graduate University of Science and Technology, Vietnam Academy Science and Technology

Supervisors:

1. Supervisor 1: Assoc. Prof. Dr. Nguyen Van Dang

2. Supervisor 2: Assoc. Prof. Dr. Nguyen Thanh Tung

Referee 1: Assoc. Prof. Dr. Trinh Xuan Hoang

Referee 2: Assoc. Prof. Dr. Do Danh Bich

Referee 3: Assoc. Prof. Dr. Nguyen Manh Thang

The dissertation will be examined by Examination Board of Graduate University of Science and Technology, Vietnam Academy of Science and Technology at 9:00 a.m, May 31, 2024.

The dissertation can be found at:

1. Graduate University of Science and Technology Library

2. National Library of Vietnam

INTRODUCTION

1. The necessary of the thesis

The group of atoms is bonded together in close order without being affected by external interaction, forming structures that are a few nanometers and smaller in size. This is called nanoclusters (atomic cluster). After nearly 80 years of development, nanoclusters are a candidate that has been receiving special research attention from scientists due to their potential applications in many fields such as spintronics, catalysis, energy storage, and toptics. At these sizes, nanoclusters will have surface effects and quantum confinement phenomena, so the chemical properties of nanoclusters are fundamentally different from their physical and chemical properties in bulk structures. For example, although Au (gold) is known to be chemically inert in bulk form, it is a potent chemically active material in nanocluster form that may catalyze a variety of processes, including CO oxidation, NO reduction, adsorption, and storage of hydrogen. Some metals in bulk structure are non-magnetic or anti-ferromagnetic substances, but at nanocluster size they show ferromagnetic properties such as Rh (rhodium) and Cr (chromium). The ability to tailor the properties of nanoclusters by changing size, shape, and composition opens up unprecedented opportunities for science and technology to explore new phenomena and synthesize new materials. Therefore, there is an increasing number of studies looking for and designing nanoclusters with new and thermodynamically stable properties not only in geometric structure but also in electronic structure, from which we can synthesize and can be easily combined by chemical methods for practical applications. Since the development of high-performance computers, the aforementioned issues have been successfully solved by simulation techniques based on the approximate solution of the Schrodinger equation of the Hamiltonian energy method. In particular, studies using the density functional theory method have results consistent with experimental results, are highly reliable, and can deepen the study of many interesting physical problems. At the same time, this is also an important, parall and suggestiv research step for experimental studies, helping to determine faster and more accurately the nanocluster structure and their physicochemical properties in accordance with the application purpose.

Recent research results show that alloy nanoclusters of noble metals (Au, Ag) doped with transition metals change their stability, enhancing their physicochemical properties such as magnetic properties, optical properties, and catalytic activity as desired. In these nanocluster systems, the valence electrons in the noble metal atoms often move freely, while the outermost electrons in the transition metal atoms mainly move localized on the transition metal atoms. Depending on the interaction between delocalized and localized electrons, the localized electrons on transition metal atoms have stronger mobility, become free electrons, and participate in the electric cloud. This is leading to significant changes in the bonding, geometric structure, and electronic structure of nanoclusters. At that point, free electrons contribute to the formation of the electronic shell as well as determination of some basic of its fundamental characteristics. Free-moving electrons in nanoclusters fill the electron shell with energy levels akin to those in an inert gas atom, and they eventually become extremely stable, resembling a superatomic structure. Furthermore, the combination of noble and transition metal atoms results in an intriguing state characterized by the optimal coexistence of free and localized electrons. To deepen a basic understanding of the principles that govern atomic and moleculer electronic interactions. The localized electrons on transition metal atoms do not contribute

or remain after partially contributing to the formation of free electron shells, depending on each specific orbital, creating magnetic and unusual catalytic properties.

Up to now, the properties of simple nanoclusters are gradually being discovered, but very little is known about the properties of complex alloy nanocluster systems, especially those made from precious and transition metals. The presence of *d*-shell electrons in these metals creates many degenerate isomers in terms of energy and electronic configuration. The problem of interaction between *s-d* or *d-d* orbitals of electrons localized on transition metal atoms and free electrons in nanoclusters still has many questions and needs to be researched and clarified. In addition, a clear understanding of the physicochemical properties of alloy nanoclusters can be applied to adjust at the atomic scale some properties of nanoclusters, such as H_2 adsorption and storage for the green energy sector and sustainable development. Recently, in the thesis of Dr. Nguyen Thi Mai of our research group, we studied the geometric structure, electronic structure, and stability of transition metal-doped semiconductor nanoclusters $Si_nMn_2^+$, cobalt oxide nanoclusters $Co_nO_m^+$, and precious doped transition metal M_nCr (M = Au, Ag, and Cu and n = 2–20); $Au_{19}M$ (M = Sc-Ni). The authors' research results have shown that cobalt oxide nanoclusters do not form electronic structures, while $Si_nMn_2^+$ nanoclusters and M_nCr nanoclusters (M = Au, Ag, Cu and n = 2–20) and $Au_{19}M$ (M = Sc–Ni) have formed electronic structures with the coexistence of the free electronic structure of the nanocluster and localized electrons on the transition metal atoms. Notably, the authors have demonstrated $Au_{19}Cr$ nanoclusters with highly symmetrical tetrahedral geometry and an electronic structure filled with 20 electrons, showing that this nanocluster is very stable. In addition, the $Au_{19}Cr$ nanocluster has 5 unpaired electrons evenly distributed on the 3*d* orbitals of the Cr atom, proving that the $Au_{19}Cr$ nanocluster is a highly active "superatom" with 5 unpaired electrons. However, the thesis still has some limitations, such as not having researched and clarified the catalytic ability of the above nanocluster systems, especially not studying and determining the kinetic states in the hydrogen bonding reaction. Stemming from the need to expand the basic understanding and application potential of the above alloy nanoclusters, we chose smaller-sized alloy nanoclusters as the research object with the expectation of bringing more interesting properties. Therefore, the title of the thesis was chosen as "*Research on the physical interaction between delocalized and localized electrons in Au_9M^{2+} (M = Sc -Ni) and Ag_nCr (n = 2-12) alloy nanocluster systems by density functional theory*".

2. The goals of the thesis

Clarifying the interactions between free electrons and localized electrons in Au_9M^{2+} (M = Sc-Ni) and Ag_nCr (n = 2-12) nanocluster systems. This is a basis on which we may observe the effects of electronic structure on the development of global geometric structures, stability, properties such as bond energy and dissociation energy, and the influence of *s-d* interaction on reaction kinetics corresponding to H_2.

3. The main research content of the thesis

In addition to the introduction, conclusion, and list of references, the main content of the thesis is presented in four chapters, specifically:

Chapter 1. Overview of alloy nanoclusters

Chapter 2. Research methods

Chapter 3. s-d electronic interactions in alloy nanocluster systems

Chapter 4. Influence of s-d interaction on the properties of alloy nanoclusters.

The main results of the thesis are three articles which is published in scientific journals under the SCIE and five articles in specialized domestic scientific journals.

CHAPTER 1. OVERIEW OF ALLOY NANOCLUSTERS

1.1. Overview of alloy nanoclusters

The group of atoms is bonded together in close order without being affected by external interaction, forming structures that are a few nanometers and smaller in size. This is called nanoclusters. Nanocluster can be homogeneous, meaning it is made of one type of atom, or it can be heterogeneous, meaning it is made of two or more different types of atoms. Heterogeneous nanoclusters made from two or more different types of atoms are called alloy nanoclusters.

Most of the early experimental research on nanoclusters involved molecules, inert gas atoms, and low-melting metals. The initial aim was to understand how the structure and general properties of matter, such as conductivity, color, and magnetism, develop when a finite number of atoms combine. Although significant progress has been made to answer some basic questions about nanoclusters, in the early stages, scientists did not anticipate the diverse and interesting properties of nanoclusters. These initial results paved the way for the scientific field of nanoclusters to develop in a way never before seen in natural materials.

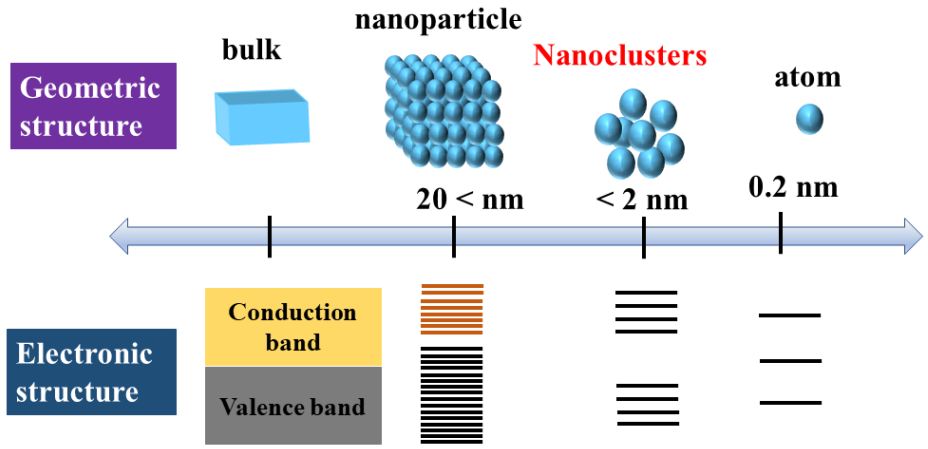

Figure 1.1. The geometric structure and electronic structure of materials depend on size.

At nanocluster size, their geometric structure, physical, and chemical properties are greatly different from their bulk form. Nanoclusters have discrete energy levels (Figure 1.1), the valence electrons on each atom in the nanocluster move freely in a potential field created by the nucleus and also form electronic shells similar to those in atoms. During the bonding process, the valence electrons in each atom move freely to the other atom, forming an electronic shell for the nanocluster with energy levels different from the electronic shell of each component atom in nanoclusters. When adding or removing only one atom in a nanocluster, it leads to sudden and unpredictable changes in the physical properties of the nanoclusters. This sudden change in the properties of nanoclusters is explained by the large number of surface atoms, resulting in a quantum confinement affect. This is a phenomenon in which the wavelength of electrons can be detected compared with particle size. This is why even a small change in the size of the nanocluster will effect the geometric structure, stability, and properties of nanoclusters. The larger sized materials (particles/nanostructure or bulk) often have a continuous energy band structure or a small band gap energy (BE, eV), corresponding to a tightly packed structure according to the law of minimizing surface area and maximzing the number of

bonds. In contrast, at nanocluster size, the changes with size are very different from those at larger sizes and difficult to predict. Therefore, nanoclusters are an object that attracts the research attention of scientists not only because of the desire to expand basic understanding of the changes in physicochemical properties of matter from the atomic level. It is also expected to design increasingly smaller and smarter materials for different applications.

CHAPTER 2. RESEARCH METHODS

The thesis uses the density functional theory method embedded in Gaussian 09 software. The Gaussview supporting software is also used to study the electronic, geometric structure, and properties of alloy nanoclusters. There are many quantum computing methods, typically the semi-empirical method, the *ab*-initio calculation method, and the density functional method. The density functional theory methods such as: BLYP, B3LYP, B3P86, B3PW91, …However, evaluating the reliability of the methods, we perform calculations to study some physical properties of small-sized nanoclusters (dimers) using the density functional theory combined with different basis set functions.

In this thesis, the electronic structure, interaction between delocalized and localized electrons, and geometric structure of Au_9M^{2+} (M = Sc-Ni) and Ag_nCr (n = 2-12) are studied using the density functional theory (DFT) method. The BP86 function combined with cc-pVTZ-pp for Au, Ag, and cc-pVTZ for transition metal M was chosen in this research. The kinetics of hydrogen adsorption on these nanoclusters were also studied at the same theoretical level, which corresponds to functional and basis sets when studying Au, Ag, and M transition metal atoms. For the H atom, we use the same function combined with the SDD basis set of functions.

CHAPTER 3. *s-d* ELECTRONIC INTERACTION IN ALLOY NANOCLUSTER SYSTEMS

3.1. *s-d* electronic interaction in Au_9M^{2+} (M = Sc-Ni) nanoclusters

3.1.1. Electronic structure of Au_9M^{2+} nanoclusters

The electronic structure of the Au_9M^{2+} nanoclusters (M = Sc-Ni) has been determined through optimized calculations using the BP86 density functional combined with the cc-pVTZ-pp and cc-pVTZ basis sets applied to the Au atom and the transition metal M atoms, respectively. The analysis reveals that the stable spin states of the Au_9M^{2+} nanoclusters range from 1 (singlet) to 6 (sextet) and depend on the remaining unpaired valence electrons in the 3*d* orbital of the respective transition metal M atoms. The highest spin state is achieved for the Au_9Cr^{2+} nanocluster (corresponding to 5 unpaired valence electrons in the 3*d* orbital of Cr), while the lowest spin state is found for the Au_9Sc^{2+} nanocluster.

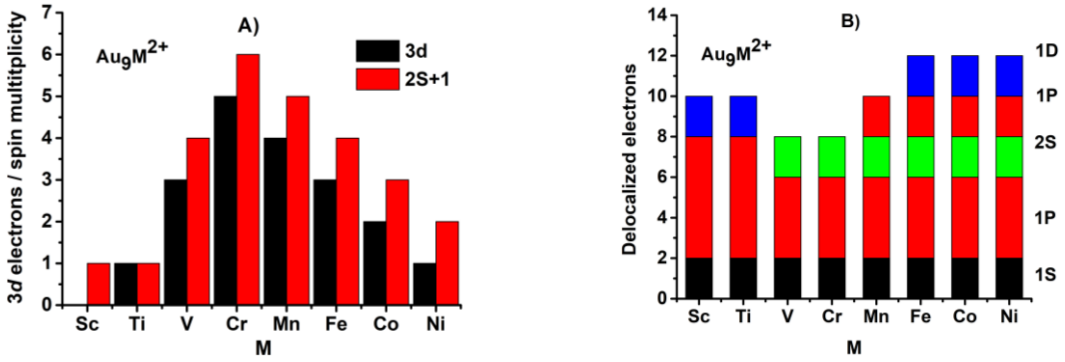

Figure 3.1. The stable spin state (2S+1), remaining unpaired valence electrons on the 3*d* orbital of transition metal M (A), and free electron shell structure of Au_9M^{2+} (M = Sc-Ni) nanoclusters (B).

The formation of the electronic structure of Au_9M^{2+} nanoclusters follows two mechanisms: (i) For Au_9Sc^{2+} and Au_9Ti^{2+} nanoclusters, the electronic structure is formed according to the closed shell rule model, based on the Jellium model related to $1S^21P^61D^2$; (ii) For Au_9M^{2+} (M = V-Ni) nanoclusters, the electronic structure is formed using the tetrahedral field rule with 20 electrons. The electrical structure of these nanoclusters then undergoes the creation of 1S shell before 1D shell becomes formed.

3.1.1. Orbitals hybridization in Au_9M^{2+} nanoclusters

The processing of doping transition metal atoms M = Sc-Ni in Au_{10}^{2+} nanoclusters leads to hybridization between the valence electrons of Au_n and the valence electrons of transition metal atoms M (*sd*-M and *s*-Au), forming the electronic structure of the Au_9M^{2+} nanoclusters. The results are shown in Table 3.1.

To clarify the hybridization process and the formation of electronic structure on each Au_9M^{2+} nanocluster, we determined the number of *sd*-M valence electrons participating in hybridization with *s*-Au valence electrons to form the electronic structure of Au_9M^{2+} nanoclusters. Following that, we build a molecular orbital energy level diagram of the Au_9M^{2+} nanocluster. The results are shown in Figure 3.2.

Table 3.1. The outermost electronic structure of transition metal M and the electronic structure of the Au_9M^{2+} (M = Sc-Ni) nanoclusters.

clusters	Valence electron M	Electronic structure	Contributing ingredients of M atoms
Au_9Sc^{2+}	$3d^14s^2$	$1S^21P^61D^2$	Sc: contributes two electrons from 4*s* orbital and one electron from 3*d* orbital.
Au_9Ti^{2+}	$3d^24s^2$	$1S^21P^61D^23d_{Ti}{}^{1\uparrow}$	Ti: contributes two electrons from 4*s* orbital and one electron from 3*d* orbital
Au_9V^{2+}	$3d^34s^2$	$1S^21P^42S^23d_V{}^{4\uparrow}$	V: contributes one electron from 4*s* orbital and one electron is excited from 4s to 3*d*
Au_9Cr^{2+}	$3d^54s^1$	$1S^21P^42S^23d_{Cr}{}^{5\uparrow}$	Cr: contributes one electron from 4*s*
Au_9Mn^{2+}	$3d^54s^2$	$1S^21P^42S^21P^23d_{Mn}{}^{4\uparrow}$	Mn: contributes two electrons from 4*s* orbital and one electrron 3*d* orbital.
Au_9Fe^{2+}	$3d^64s^2$	$1S^21P^42S^21P^21D^23d_{Fe}{}^{3\uparrow}$	Fe: contributes two electrons from 4*s* orbital and three electrons from 3*d* orbital.
Au_9Co^{2+}	$3d^74s^2$	$1S^21P^42S^21P^21D^23d^23d_{Co}{}^{2\uparrow}$	Co: contributes two electrons from 4*s* orbital and three electrons from 3*d* orbital.
Au_9Ni^{2+}	$3d^84s^2$	$1S^21P^42S^21P^21D^23d^43d_{Ni}{}^{1\uparrow}$	Ni: contributes two electrons from 4*s* orbital and three electrons from 3*d* orbital.

It can be seen that the formation of the electronic structure of Au_9M^{2+} nanoclusters is the result of the hybridization process between the valence electrons *sd*-M and *s*-Au. The hybridization between the 6*s* valence electrons of the Au atoms and the total or partial valence electrons of the 3*d* and 4*s*-M transition metal atoms in the Au_9M^{2+} nanoclusters will form two types of electronic states. The shared valence electrons move freely, forming the electronic structure of the nanoclusters. However, the remaining valence electrons on the M atoms do not contribute to the formation of the electronic structure. It will be localized and evenly distributed on the 3*d* orbital of the transition metal atom M. The number of unpaired localized electrons in the 3*d* orbitals of the transition metal atom M depends on the dopant atom. For Au_9Sc^{2+} nanocluster, all three valence electrons of Sc (two 3*d* and one 4*s*

electrons) contribute to the seven valence electrons of Au_9^{2+} nanocluster to form the $1S^21P^61D^2$ electronic structure. In contrast, only one 4*s* valence electron of the Cr atom attends to the free electron cloud of Au_9Cr^{2+} nanocluster, the remaining five valence electrons on 3*d*-M. It is these localized electrons that determine the magnetic properties and catalytic ability of Au_9M^{2+} nanoclusters. Thus, Au_9M^{2+} nanoclusters have a stable electronic structure and strong catalytic potential.

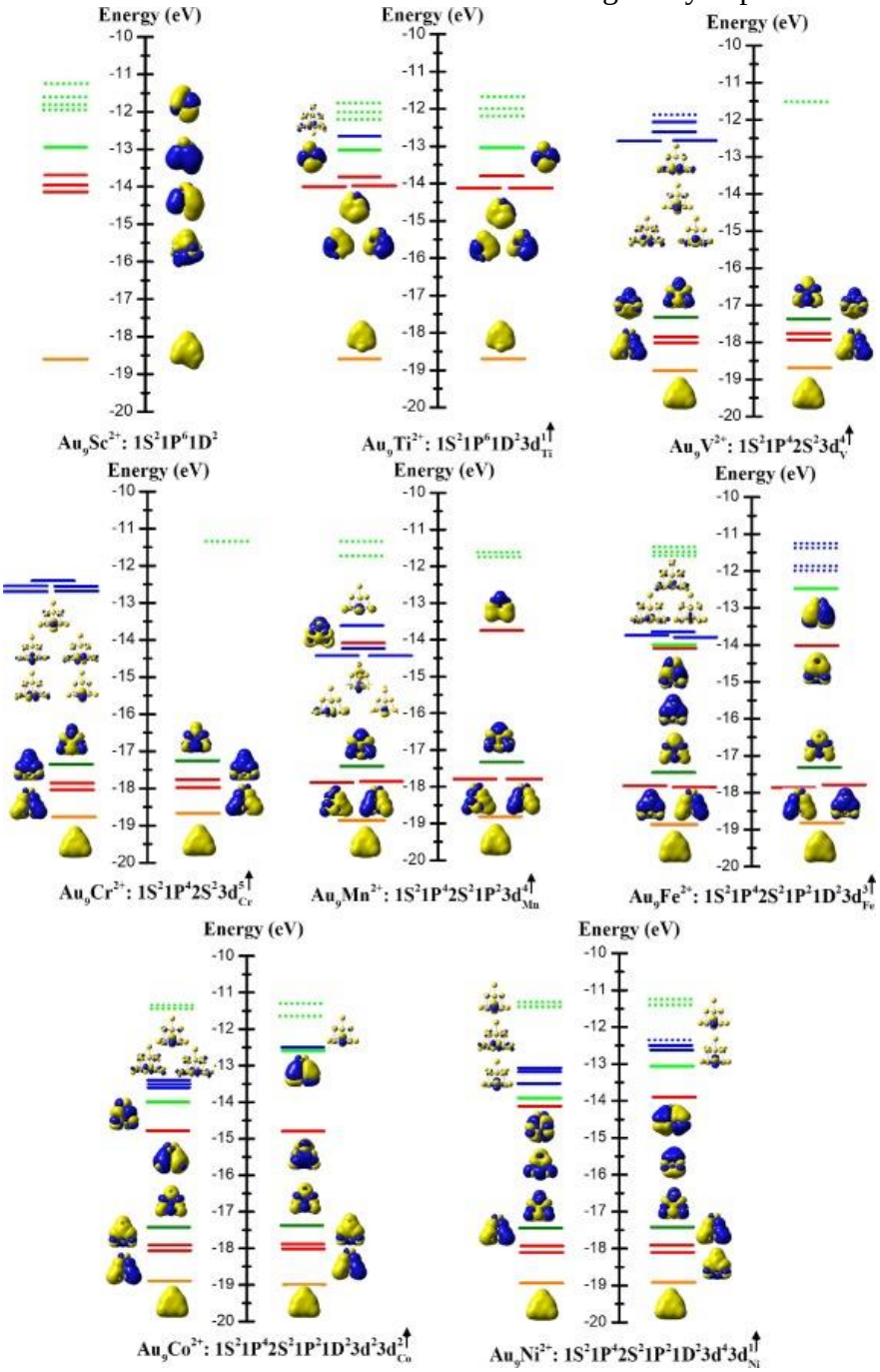

Figure 3.2. Molecular orbital energy level diagram of the Au_9M^{2+} (M = Sc-Ni) nanoclusters with images of molecular orbitals and 3*d* orbitals localized on the M atom.

3.1.3. Desity of electronic states on Au_9M^{2+}nanoclusters

To study the electronic structure corresponding to energy levels as well as bond formation in Au_9M^{2+} (M = Sc-Ni) nanoclusters, we analyze and compare the total state density distribution and partial density of states. It can be seen that the coexistence of free electronic structure and localized electrons at their energy positions in the Au_9M^{2+} nanocluster, resulting of hybridization between *sd*-M

and *s*-Au electrons. The 1S, 2S, 1P, and 1D subshells are located in different respective energy regions and form from the interaction between the *sd*-M and *s*-Au orbitals. The HOMO of Au_9M^{2+} nanoclusters contains unpaired electrons, suggesting that these nanoclusters have potential for catalytic processes.

3.2. *s-d* electronic interaction in Ag_nCr (n = 2-12) nanoclusters

3.2.1. Electronic structure of Ag_nCr nanoclusters

The results of analyzing the stable spin state of Ag_nCr nanoclusters fluctuate between two states (5 (quintet) and 6 (sextet) for small-sized nanoclusters ($n \leq 5$) and It depends on the number of unpaired valence electrons 3*d*-Cr. In contrast, the number unpaired 3*d* valence electrons of Ag_nCr nanoclusters tends to decrease at the larger than n = 6-12, corresponding to the spin state of Ag_nCr 7 (septet) at n = 6 and 1 (singlet) at n = 12 (Figure 3.4A).

The electronic structure of Ag_nCr nanoclusters is formed according to the 18-electron rule and reaches a filled electronic configuration at size n = 12 corresponding to $1S^21P^61D^{10}$ (Figure 3.4B).

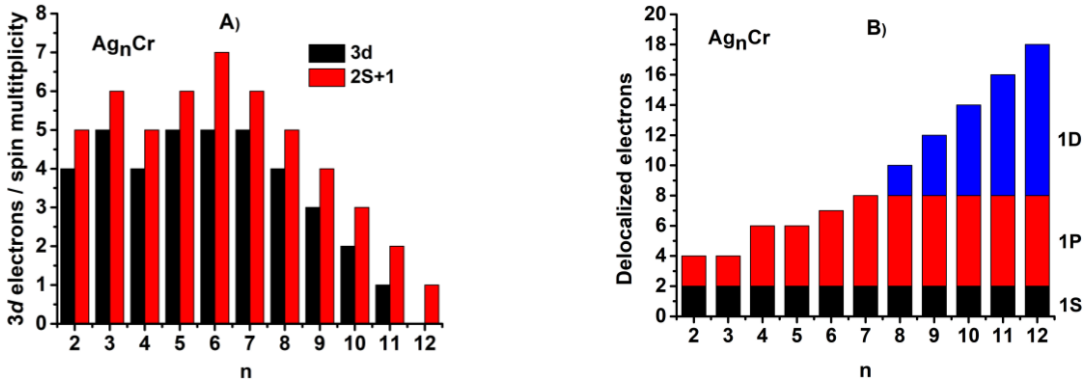

Hình 3.4. The stable spin state (2S+1), remaining unpaired valence electrons on the 3*d* orbital of Cr atom (A), and free electron shell structure of Ag_nCr (n = 2-12) nanoclusters (B).

3.2.2. Orbitals hybridization in Ag_nCr nanoclusters

The dopant Cr atom in Ag_n nanoclusters leads to hybridization between *sd*-M and *s*-Ag, forming the electronic structure of Ag_nCr nanoclusters. The results are presented in Table 3.2 and Figure 3.5.

Table 3.2. Electronic structure of Ag_nCr (n = 2-12) nanoclusters.

Nanoclusters	**Electronic structure of Ag_nCr**	**Contributing ingredients of Cr atom**
Ag_2Cr	$1S^21P^23d^{4\uparrow}$	Cr: contributes one electron from 3*d* orbital and one electron from 4*s* orbital.
Ag_3Cr	$1S^21P^23d^{5\uparrow}$	Cr: contributes one electron from 4*s* orbital.
Ag_4Cr	$1S^21P^43d^{4\uparrow}$	Cr: contributes one electron form 3*d* orbital and one electron from 4*s* orbital.
Ag_5Cr	$1S^21P^43d^{5\uparrow}$	Cr: contributes one electron form 4*s* orbital.
Ag_6Cr	$1S^21P^43d^{5\uparrow}1P^{1\uparrow}$	Cr: contributes one electron from 4*s* orbital.
Ag_7Cr	$1S^21P^63d^{5\uparrow}$	Cr: contributes one electron from 4*s* orbital.
Ag_8Cr	$1S^21P^61D^23d^{4\uparrow}$	Cr: contributes one electron from 3*d* orbital and one electron form 4*s* orbital.
Ag_9Cr	$1S^21P^61D^43d^{3\uparrow}$	Cr: contributes two electrons from 3*d* orbital and one electron form 4*s* orbital.
$Ag_{10}Cr$	$1S^21P^61D^63d^{2\uparrow}$	Cr: contributes three electrons from 3*d* orbital and one electron form 4*s* orbital.

$Ag_{11}Cr$	$1S^21P^61D^83d^{1\uparrow}$	Cr: contributes four electrons from 3*d* orbital and one electron from 4*s* orbital.
$Ag_{12}Cr$	$1S^21P^61D^{10}$	Cr: contributes five electrons form 3*d* orbital and one electron form 4*s* orbital.

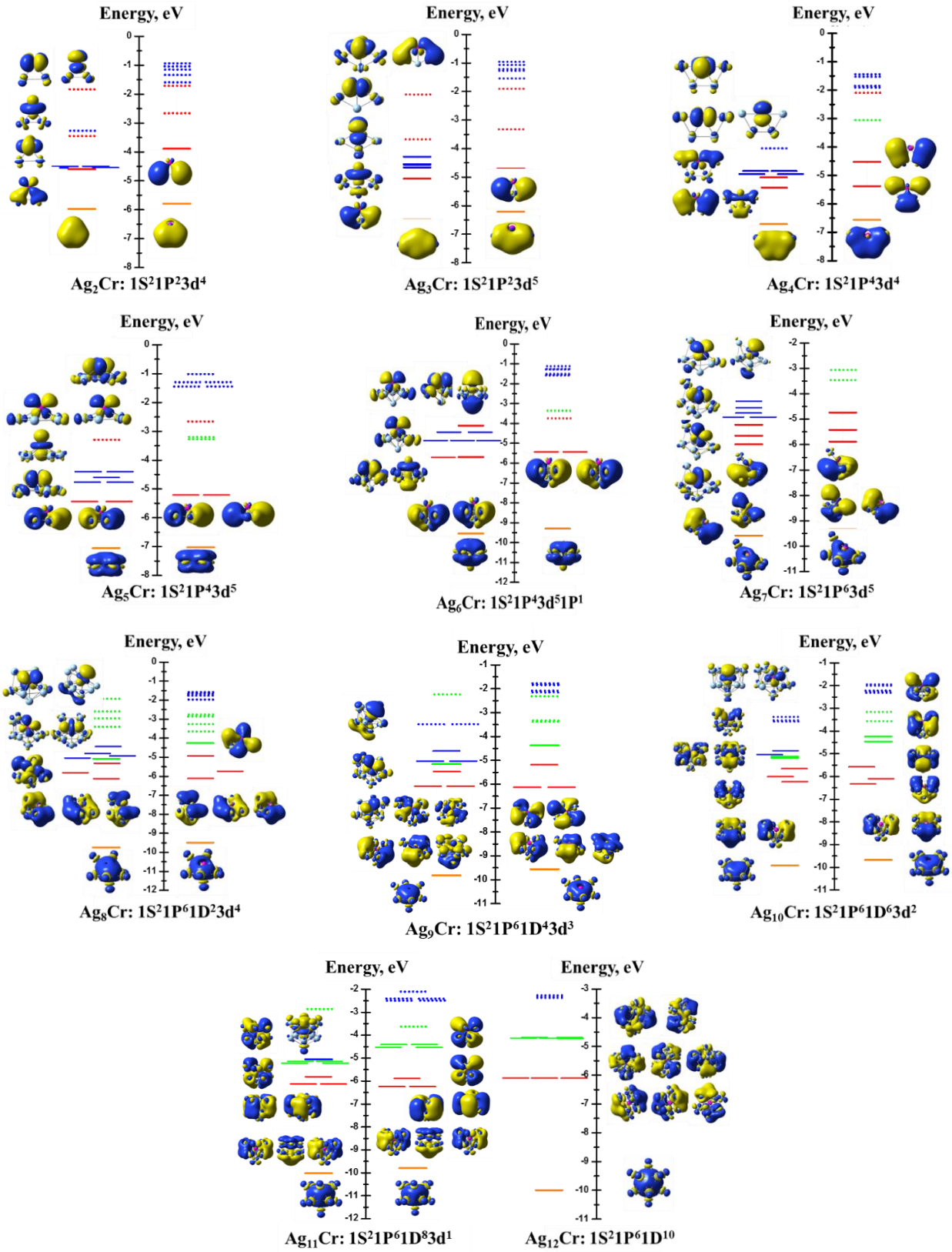

Figure 3.5. Molecular orbital energy levels distribution diagram of Ag_nCr (n = 2-12) nanocluster with images of molecular orbitals and localized 3*d* orbitals.

The rules of formation and development of the electronic structure of Ag_nCr nanoclusters in Table 3.2 and Figure 3.5 show that the valence electrons $5s^1$ of Ag atoms and $4s^1$ of Cr atoms tend to move freely, participating in forming the electronic shell of Ag_nCr nanoclusters. Depending on the size of the nanocluster, 3*d*-Cr valence electrons contribute partially or completely to the free electron shell of the nanocluster. The remaining electrons on the Cr atom tend not to pair and move locally, localized in their own 3*d* orbitals. The coexistence of free electronic structure and localized electrons on transition metal atoms in electronic structure shows that these nanoclusters have catalytic potential.

3.2.3. Desity of electronic states on Ag_nCr nanocluster

To understand clearly the electronic structure as well as have a more intuitive view of the distribution of electronic states along with energy levels and bond states in each Ag_nCr (n = 2-12) nanocluster, we analyze the total density of states (DOS) and partial density of states (pDOS) corresponding to the energy level of Ag_nCr (n = 2-12) nanoclusters.

The distribution of the total density of states (DOS) and partial density of states (pDOS) is approximately -8 ÷ 0 eV at small sizes $n \leq 5$. However, this distribution is in the range of -11 ÷ -2 eV at bigger scales. The interaction between *sd*-Cr and *s*-Ag electrons forms 1S, 1P, and 1D subshells, which are confined at distinct energy levels, depending on the size of the nanocluster. At size n = 6, the 1P orbital exhibits energy degeneracy and is located at a lower energy level compared to smaller nanoclusters. Additionally, the analysis of orbital state distribution indicates that the $5s^1$ valence electron of Ag and the $4s^1$ valence electron of Cr tend to move freely and participate in the formation of a shared electron shell for the Ag_nCr nanocluster. In contrast, the 3*d* electrons of the impurity phase Cr atom, depending on the size of the nanocluster, contribute partially/totaly to the free-moving electron shell of the nanocluster. The interaction between these orbitals creates bonding states within the nanocluster, influencing the geometric structure and stability of these nanoclusters. The remaining 3*d* electrons on the Cr atom do not contribute to the shared electron cloud and tend to be unpaired and distributed in the HOMO state, affecting the catalytic properties of Ag_nCr nanoclusters.

3.3. Conclusion of Chapter 3

In Chapter 3, we used the density functional theory method with the BP86 functional in conjunction with the cc-pVTZ-pp and cc-pVTZ basis sets. These were employed respectively for the noble metal atoms (Au, Ag) and the transition metal atom M to determine the physical interactions between delocalized and localized electrons in two nanocluster systems:

i) By maintaining a constant number of *s* valence electrons and adjusting the valence electron count through variations in the impurity atoms within the Au_9M^{2+} nanocluster systems (M = Sc-Ni).

ii) By altering the size of the host nanocluster, resulting in changes in the number of *s* valence electrons while retaining the valence electron count of the impurity Ag_nCr atoms (n = 2-12).

The results show that the *s-d* electrons interaction strongly depends on the size and composition of the nanoclusters. The dopant of transition metal impurity atoms into noble metal nanoclusters leads to the coexistence of the nanocluster's free electron shell structure and the localized unpaired electrons on the transition metal atoms. The remaining valence electrons of the transition metal atoms do not contribute to the free electron cloud motion of the nanoclusters; instead, they remain unpaired and localized on their own 3*d* orbitals. The number of unpaired valence electrons localized on the 3*d* orbitals of the transition metal atoms depends on the composition and size of the nanoclusters. These unpaired electrons create an ideal interaction environment for electron-related

properties, such as catalytic behavior in alloy nanoclusters. Additionally, the research findings on the *s-d* electron interaction also provide information for predicting the geometric structure and stability of the aforementioned nanoclusters.

CHAPTER 4. INFULENCE OF *s-d* INTERACTION ON THE PROPERTIES OF ALLOY NANOCLUSTERS

4.1. Au_9M^{2+} (M = Sc–Ni) nanoclusters

4.1.1.The geometric structure of Au_9M^{2+} nanoclusters

The optimized geometric structures are presented in Figure 4.1. The symbols a.M.b/n^m correspond to a where it represents the number of gold atoms, M ranging from Sc to Ni, b representing the stable isomers of the Au_9M^{2+} nanoclusters (denoted as A, B, and C), and n indicating the relative energy value of the isomer compared to the most stable one (in eV). The value m corresponds to the spin multiplicity.

The stable geometric structures of the Au_9M^{2+} nanoclusters (M = Sc, Ti) exhibit a cage-like structure, with the impurity atom replacing one gold atom at a high coordination site. Conversely, for heavier impurity atoms (M = V-Ni), the stable geometric structure of the Au_9M^{2+} nanoclusters tends to retain the tetrahedral structure of the Au_{10}^{2+} nanocluster. In this case, the impurity atom is substituted at the edge of this structure.

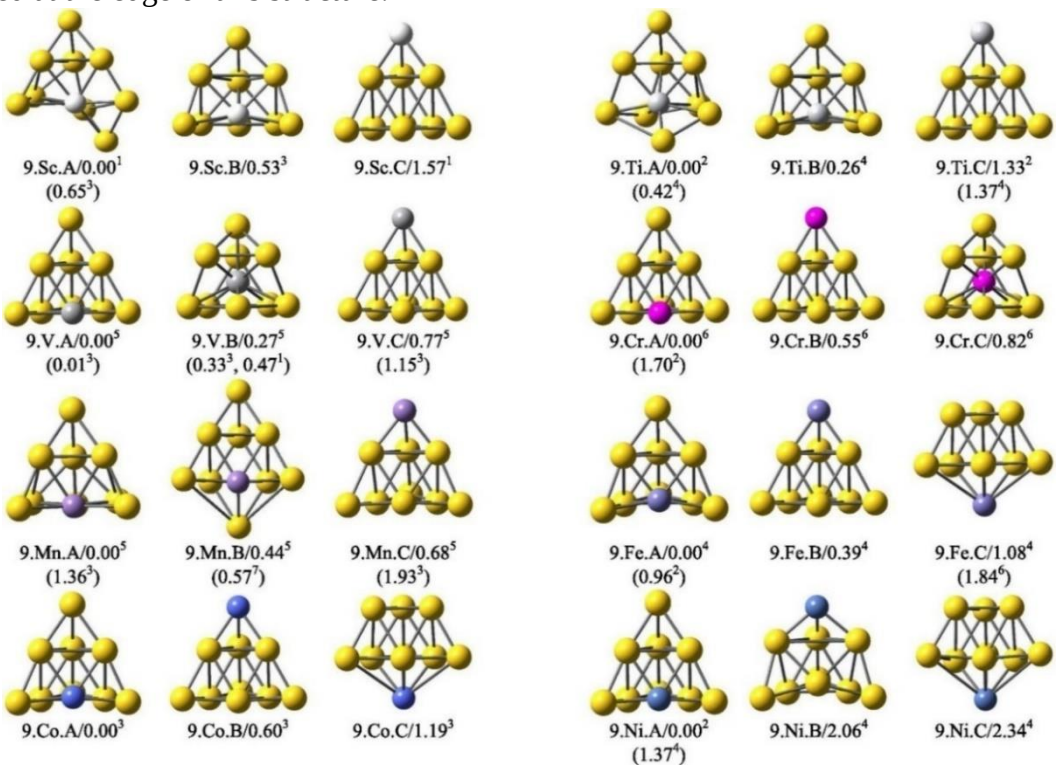

Figure 4.1. The geometric structure of Au_9M^{2+} (M = Sc-Ni) nanoclusters, in which white, gray, dark gray, magenta, purple, violet, light blue, dark blue, and yellow correspond to the Sc, Ti, V, Cr, Mn, Fe, Co, Ni, and Au elements, respectively.

4.1.2. The stability of Au_9M^{2+} nanoclusters

4.1.2.1. The average binding energy of Au_9M^{2+} nanoclusters

The average binding energy (*BE*, eV) of Au_{10}^{2+} and Au_9M^{2+} nanoclusters are determined following:

$$BE(Au_n^{2+}) = \frac{1}{n}[(n-2)E(Au) + 2E(Au^+) - E(Au_n^{2+})] \quad (4.2)$$

$$BE(Au_{n-1}M^{2+}) = \frac{1}{n}[(n-3)E(Au) + 2E(Au^+) + E(M) - E(Au_{n-1}M^{2+})] \quad (4.3)$$

Where $E(Au)$, $E(Au^+)$, $E(Au_n^{2+})$, $E(M)$, and $E(Au_{n-1}M^{2+})$ respectively represent the total energy of nanoclusters in their ground states. The results are presented in Figure 4.3.

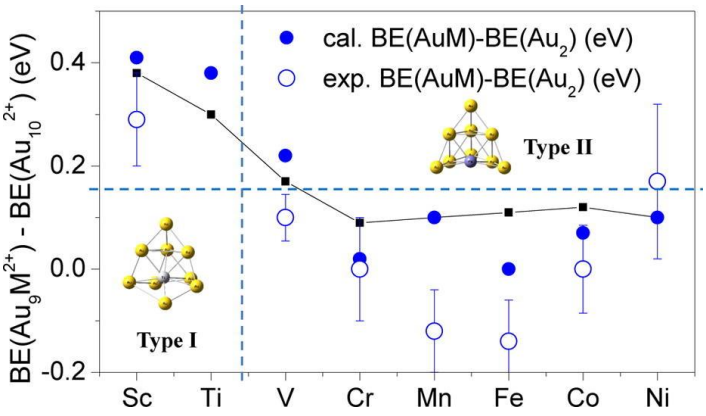

Figure 4.3. The average bond energy differences between AuM and Au_2; Au_9M^{2+} and Au_{10}^{2+} (M = Sc-Ni).

Where $E(Au)$, $E(Au^+)$, $E(Au_n^{2+})$, $E(M)$, and $E(Au_{n-1}M^{2+})$ respectively represent the total energy of nanoclusters in their ground states. The analysis of the bond energy (BE) reveals that the BE values of the Au_9M^{2+} nanoclusters are generally higher than those of the Au_{10}^{2+} nanocluster, indicating that the dopant transition metal atoms enhances the stability of the nanoclusters.

4.1.2.2. The dissociation energy of Au_9M^{2+} nanoclusters

The dissociation energy of Au_9M^{2+} (M = Sc-Ni) is determined by:

$Au_9M^{2+} \rightarrow Au_7M^{2+} + Au_2$ (4.4) $Au_9M^{2+} \rightarrow Au_8^{2+} + AuM$ (4.5) $Au_9M^{2+} \rightarrow Au_9^{2+} + M$ (4.6)

$Au_9M^{2+} \rightarrow Au_8M^{2+} + Au$ (4.7) $Au_9M^{2+} \rightarrow Au_9^{+} + M^{+}$ (4.8) $Au_9M^{2+} \rightarrow Au_9 + M^{2+}$ (4.9)

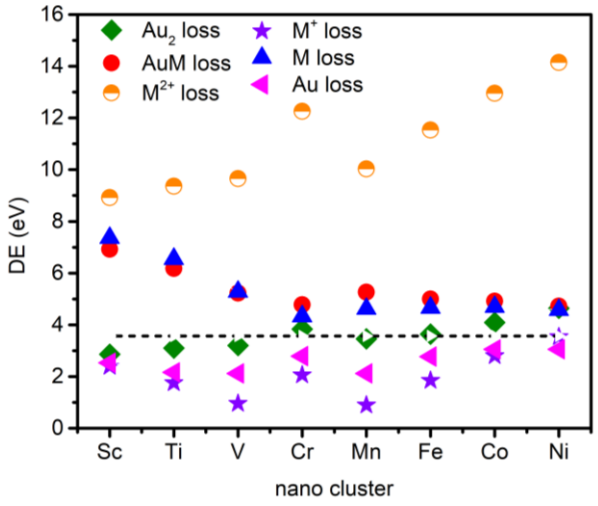

Figure 4.4. Dissociation energy (*DE*, eV) of Au_9M^{2+} (M = Sc-Ni) nanoclusters according to dissociation channels (4.4) → (4.9).

Where M represents a transition metal atom (M = Sc-Ni). The results are presented in Figure 4.4.This analysis of the bond dissociation energy reveals a preference for cleavage towards the Au atom and the Au_2 molecule in terms of energy. Conversely, cleavage towards the transition metal atom M and the AuM molecule is not energetically favored. It is worth noting that the bond

dissociation energies in all four cleavage directions for the Au_9Cr^{2+} nanocluster are high, indicating its high stability. This predicts its potential as a promising superatom, making it highly suitable for fabrication and synthesis using experimental techniques.

4.1.3. Hydrogen adsorption process on Au_9M^{2+} (M = Sc-Ni) nanoclusters

4.1.3.1. The geometric structure of $Au_9M^{2+}@H_2$ nanoclusters

The stable geometric structures of Au_9M^{2+} (M = Sc-Ni) nanoclusters adsorbing H_2 were calculated using the B3LYP functional combined with the cc-pVTZ-pp, cc-pVTZ, and SDD basis sets for Au, M, and H atoms, respectively. Two adsorption forms were observed: molecular adsorption of Au_9M^{2+}-H_2 and atomic adsorption of Au_9M^{2+}-2H (M = Sc-Ni). The results are presented in Figure 4.5.

The analysis of the stable geometric structures of $Au_9M^{2+}@H_2$ nanoclusters reveals that the adsorption positions of H_2 molecules can be divided into two groups. In the first group, for Au_9V^{2+} and Au_9Ni^{2+} nanoclusters, hydrogen molecules tend to adsorb on the surface transition metal atoms V and Ni. In the second group, hydrogen molecules prefer to adsorb on a gold atom at the vertex of a tetrahedral structure for the dopant atoms M = Sc, Ti, Cr, Mn, Fe, and Co. Regarding the bond dissociation adsorption cases, we generally observe two positions for H_2 adsorption. The first position is the bridge position between two gold atoms at the vertex, where the dopant atoms are encapsulated with gold atoms (M = Sc, Ti, and Mn). The second position involves an Au-M position and an Au-Au position, where one dopant atom is located at the edge (M = V, Cr, Co, and Ni). Notably, for the Au_9Fe^{2+}-2H nanocluster, the Fe dopant atom is also located at the edge position, but both H atoms bond to bridge positions between Au-Au atoms.

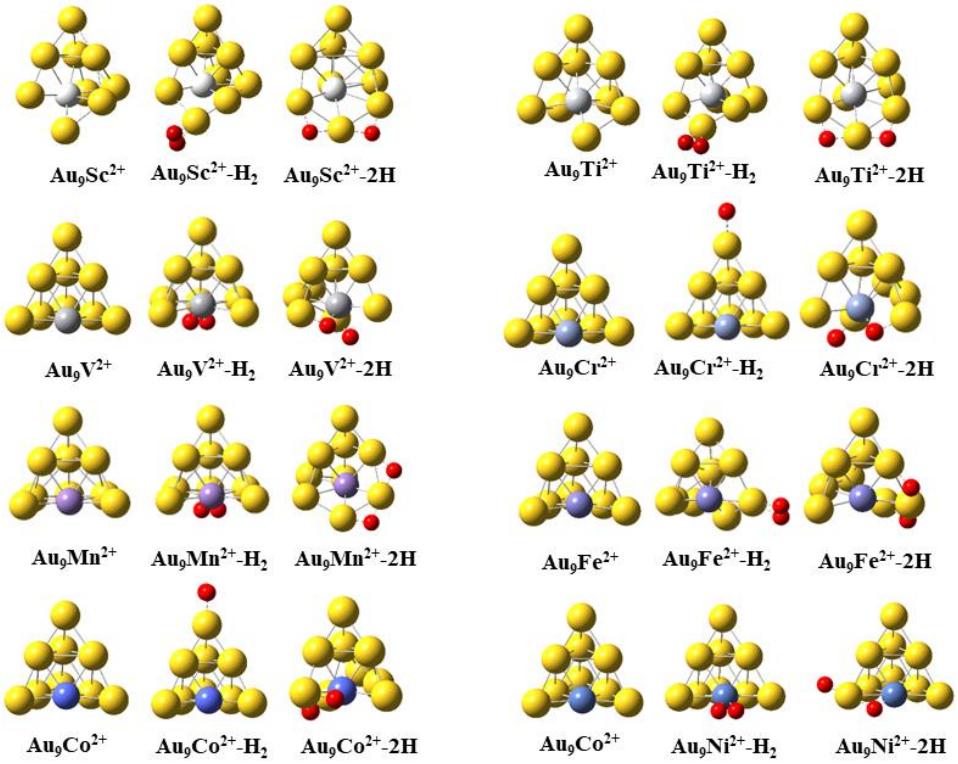

Figure 4.5. The optimized geometric structures of Au_9M^{2+}, Au_9M^{2+}-H_2, and Au_9M^{2+}-2H (M = Sc-Ni) nanoclusters are shown. The yellow represents Au atoms, while red represents H atoms. The colors white, gray, dark gray, magenta, purple, violet, light blue, dark blue, and yellow correspond to the elements Sc, Ti, V, Cr, Mn, Fe, Co, Ni, and Au, respectively.

4.1.3.2. The stability of $Au_9M^{2+}@H_2$ nanoclusters

The stability of $Au_9M^{2+}@H_2$ nanoclusters is determined by calculating the average bond energy values bình (*BE*, eV) based on equations 4.8 and 4.9.

$$BE(Au_9M^{2+}H_2) = \frac{1}{12}[7E(Au) + 2E(Au^+) + E(M) + 2E(H) - E(Au_9M^{2+}H_2)] \quad (4.8)$$

$$BE\ (Au_9M^{2+} - 2H) = \frac{1}{12}[7E(Au) + 2E(Au^+) + E(M) + 2E(H) - E(Au_9M^{2+} - 2H)] \quad (4.9)$$

Where *E* is the total energy of nanoclusters and atoms. The results are shown in Figure 4.6.

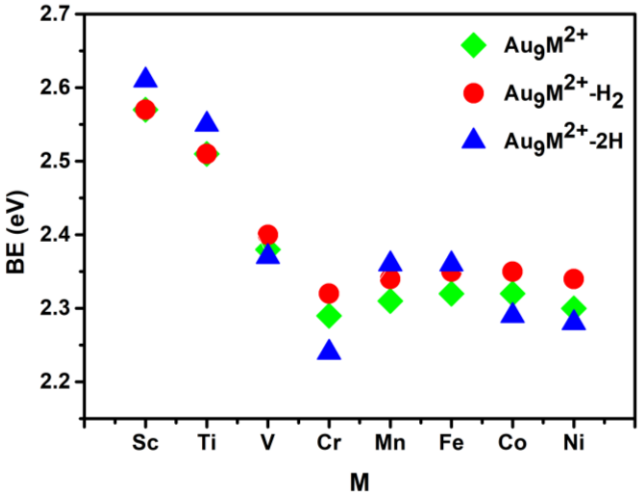

Figure 4.6. The average binding energy (*BE*, eV) of Au_9M^{2+}, Au_9M^{2+}-H_2, and Au_9M^{2+}-2H (M = Sc-Ni) nanoclusters.

4.1.3.3. Kinetic state of Au_9M^{2+} nanocluster during binding with H_2

In order to gain fundamental understanding of the H_2 adsorption process on Au_9M^{2+} nanoclusters, we calculated the adsorption energy and the H-H bond length for both molecular adsorption and atomic adsorption of two hydrogen atoms. These calculations were performed using equations 4.10 and 4.11, respectively.

$$E_{ads}(Au_9M^{2+} - H_2) = E(Au_9M^{2+}) + E(H_2) - E(Au_9M^{2+} - H_2) \quad (4.10)$$

$$E_{ads}(Au_9M^{2+} - 2H) = E(Au_9M^{2+}) + E(H_2) - E(Au_9M^{2+} - 2H) \quad (4.11)$$

The calculated results are presented in Table 4.3.

Table 4.3. The adsorption energy (E_{ads}, eV) and the H-H bond length (d_{H-H}, Å) of Au_9M^{2+}-H_2 and Au_9M^{2+}-2H (M = Sc-Ni) nanoclusters.

M	**E_{ads}/eV**		**d_{H-H}/Å**	
	$Au_9M^{2+}H_2$	**Au_9M^{2+}-2H**	**Au_9M^{2+}-H_2**	**Au_9M^{2+}-2H**
Sc	0.34	0.87	0.79	3.50
Ti	0.44	0.95	0.79	3.50
V	0.41	0.04	0.82	3.22
Cr	0.32	-0.67	0.79	3.60
Mn	0.32	0.52	0.80	3.54
Fe	0.32	0.51	0.79	3.56
Co	0.34	-0.33	0.79	3.53
Ni	0.38	-0.33	0.81	3.41

Table 4.3 shows that the H-H bond length (d_{H-H}) in Au_9M^{2+}-H_2 nanoclusters (0.79 Å to 0.82 Å) is significantly elongated compared to the bond length of the H_2 molecule (0.75 Å), indicating activation of H_2 upon adsorption. On the other hand, the distances between the two hydrogen atoms

in Au_9M^{2+}-2H nanoclusters range from 3.22 Å to 3.60 Å, suggesting complete dissociation of H_2 on the surface of the nanocluster. Comparing the adsorption energies of the molecular adsorption and atomic adsorption processes, it can be observed that the formation of Au_9M^{2+}-H_2 is preferred. Conversely, Au_9Cr^{2+}-2H, Au_9Co^{2+}-2H, and Au_9Ni^{2+}-2H nanoclusters exhibit negative E_{ads} values, indicating that the atomic adsorption of H_2 on these nanoclusters is exothermic and less favorable to occur.

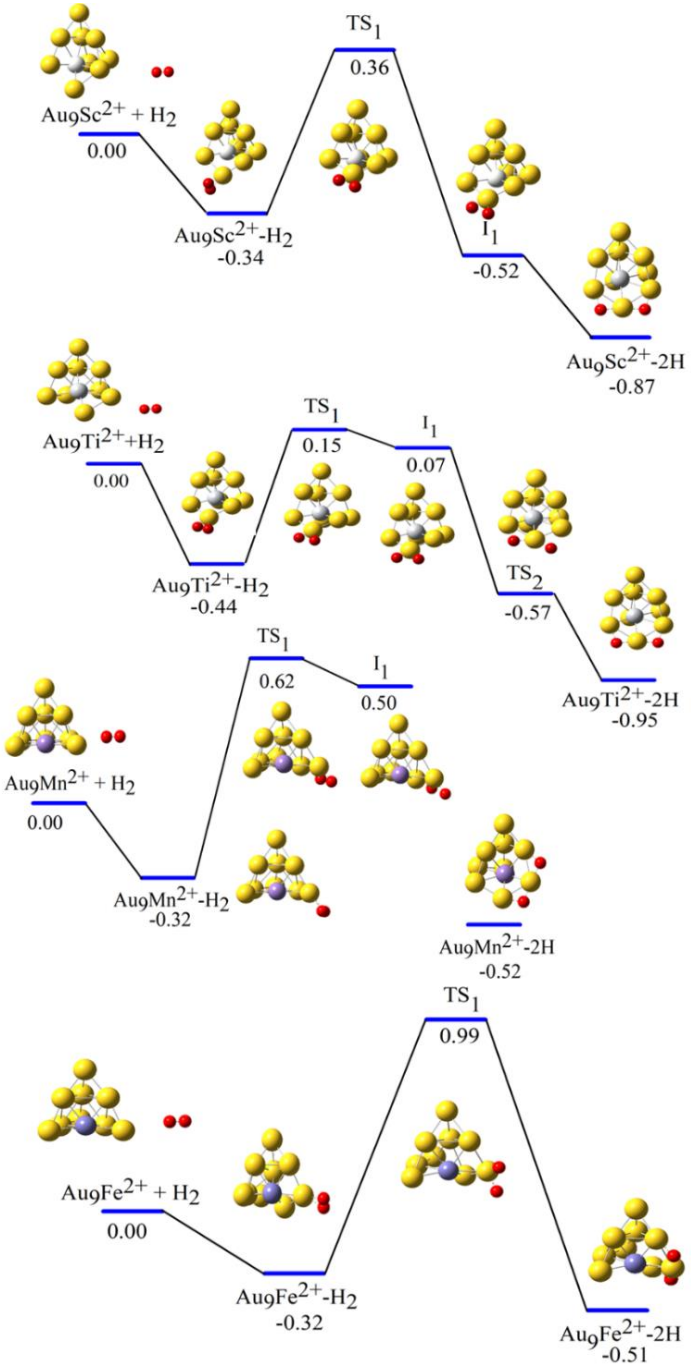

Figure 4.9. The calculated reactions pathways and relative free energies (in eV) for molecular adsorption and atomic adsorption of H_2 on Au_9M^{2+}-2H (M = Sc, Ti, Mn, Fe) nanoclusters.

To investigate the nature of hydrogen bonding adsorbed on Au_9M^{2+} nanoclusters, we conducted calculations of the partial density of states (pDOS) and total density of states (DOS) for the adsorbed nanoclusters in both molecular hydrogen adsorption form Au_9M^{2+}-H_2, and atomic hydrogen adsorption form Au9M2+-2H.

To gain a deeper understanding of the dissociative adsorption mechanism of Au_9M^{2+} nanoclusters (M = Sc, Ti, Mn, and Fe), we determined the interaction pathways of hydrogen with these nanoclusters. Figure 4.8 illustrates the calculated reaction pathways and relative free energies (in eV) for the molecular adsorption and dissociation of H_2 on Au_9M^{2+}-2H nanoclusters with M = Sc, Ti, Mn, and Fe.

The analysis results in Figure 4.9 show that, although the final products of the H_2 dissociation process on Au_9Sc^{2+}, Au_9Mn^{2+}, and Au_9Fe^{2+} nanoclusters have relatively low energies of -0.87 eV, -0.95 eV, -0.52 eV, and -0.51 eV, respectively. Compared to their corresponding channels, there are still energy barriers of 0.36 eV, 0.62 eV, and 0.99 eV, respectively, to activate the H_2 dissociation process for molecular adsorption on the nanoclusters. This suggests that the molecular adsorption of H_2 is favorable for these nanoclusters, but the H_2 dissociation process is unlikely to occur without external stimuli, especially for Au_9Mn^{2+} and Au_9Fe^{2+} nanoclusters. In contrast, the Au_9Ti^{2+} nanoclusters require an activation energy of 0.15 eV for the dissociation process, indicating hydrogen storage potential.

The mechanism regarding the influence of *s-d* interaction on the stable geometric structure of Au_9M^{2+} (M = Sc-Ni) and the adsorption of hydgrogen on Au_9M^{2+} nanoclusters is presented in Table 4.4.

Table 4.4. The influence of *s-d* interaction on the geometric structure of Au_9M^{2+} (M = Sc-Ni) nanoclusters and their interaction with H_2.

M	**Valence electrons on M**	**Electronic structure of Au_9M^{2+}**	**Electronic strcutrure components of Au_9M^{2+}**	**Geometric structure of Au_9M^{2+}**	**E_{ads}, eV**		**Activation energies barrier, eV**
					Au_9M^{2+}-H_2	**Au_9M^{2+}-2H**	
Sc	$3d^14s^2$	$1S^21P^61D^2$	Sc: contributes 2 electrons from the 4*s* orbital and 1 electron from the 3*d* orbital.		0.34	0.87	0.70
Ti	$3d^24s^2$	$1S^21P^61D^23d_{Ti}^{1\uparrow}$	Ti: contributes 2 electrons from the 4*s* orbital and 1 electron from the 3*d* orbital.	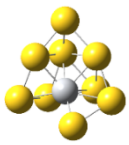	0.44	0.95	0.59
V	$3d^34s^2$	$1S^21P^42S^23d_{V}^{4\uparrow}$	V: contributes 1 electron from the 4*s* orbital and 1 electron is excited to 3*d* orbital.	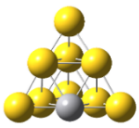	0.41	0.04	-
Cr	$3d^54s^1$	$1S^21P^42S^23d_{Cr}^{5\uparrow}$	Cr: contributes 1 electron from the 4*s* orbital.	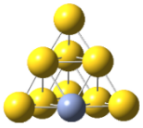	0.32	-0.67	-
Mn	$3d^54s^2$	$1S^21P^42S^21P^23d_{Mn}^{4\uparrow}$	Mn: contributes 2 electrons from the 4*s* orbital and 1 electron from 3*d* orbital.	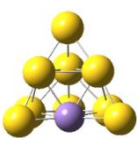	0.32	0.52	0.94

Fe	$3d^6 4s^2$	$1S^2 1P^4 2S^2 1P^2 1D^2 3d_{Fe}{}^{3\uparrow}$	Fe: contributes 2 electrons from the 4*s* orbital and 3 electrons from the 3*d* orbital.	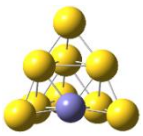	0.32	0.51	1.31
Co	$3d^7 4s^2$	$1S^2 1P^4 2S^2 1P^2 1 D^2 3d^2 3d_{Co}{}^{2\uparrow}$	Co: contributes 2 electrons from the 4*s* orbital and 3 electrons from the 3*d* orbital.	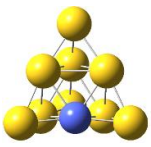	0.34	-0.33	-
Ni	$3d^8 4s^2$	$1S^2 1P^4 2S^2 1P^2 1 D^2 3d^4 3d_{Ni}{}^{1\uparrow}$	Ni: contributes 2 electrons from the 4*s* orbital and 3 electrons from the 3*d* orbital.	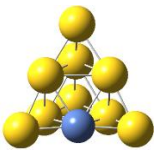	0.38	-0.33	-

4.2. Ag_nCr (n = 2-12) nanoclusters

4.2.1. The geometric structure of Ag_nCr nanoclusters

The results of analyzing the development of the stable geometric structures of Ag_nCr nanoclusters (n = 2-12) are presented in Figure 4.14.

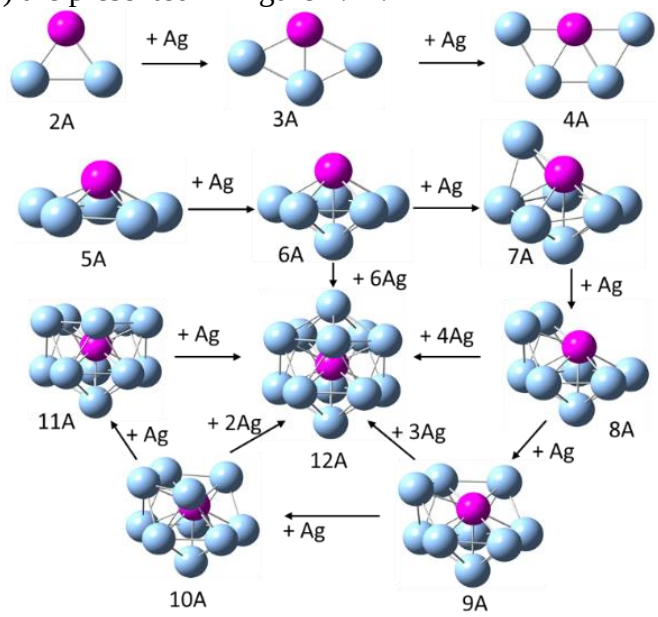

Figure 4.14. The growth of geometric structure of Ag_nCr (n = 2-12) nanoclusters.

For nanoclusters with small sizes ($n \leq 5$), the stable geometric structure of Ag_nCr nanoclusters is in a 2D form. In contrast, for larger sizes (n = 6-12), the stable geometric structure of Ag_nCr nanoclusters is three-dimensional. The transition from a 2D to a 3D structure occurs at n = 6. The Cr atoms are doped into noble metal nanoclusters with a tendency to occupy positions with the highest coordination numbers, forming multiple bonds with the underlying Ag_n nanoclusters.

4.2.2. The stability of Ag_nCr nanoclusters

The relative stability of Ag_nCr nanoclusters is determined through the analysis of avarage binding energy (*BE*, eV), second-order bond energy difference ($\Delta_2 E$, eV), and dissociation energy (*DE*, eV).

4.2.2.1. The average binding energy of Ag_nCr nanoclusters

The average binding energy (*BE*, eV) of Ag_nCr nanocluster is calculated by:

$$BE(Ag_nCr) = \frac{1}{n+1}[(E(Cr) + nE(Ag)) - E(Ag_nCr)] \quad (4.12)$$

$$BE(Ag_{n+1}) = \frac{1}{n+1}[(n+1)E(Ag)) - E(Ag_{n+1})] \quad (4.13)$$

The results are shown in Figure 4.11.

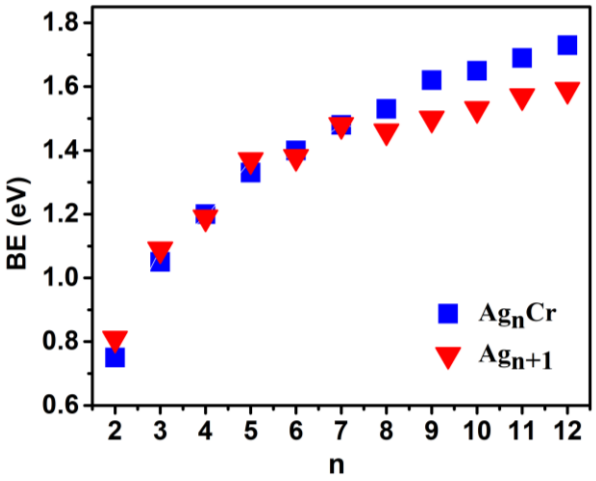

Figure 4.11. The average binding energy (*BE*, eV) of Ag_nCr and Ag_{n+1} (n = 2-12) nanoclusters.

The analysis BE of Ag_nCr nanoclusters reveals two distinct regions. For small-sized $n \leq 7$ nanoclusters, *BE* values are lower compared to the BE of Ag_{n+1} nanoclusters. In contrast, for larger size n = 8-12, the *BE* of Ag_nCr nanoclusters are significantly higher than those of Ag_{n+1} nanoclusters, particularly at n=12.

4.2.2.2. The second-order bond energy difference

The second-order bond energy difference of Ag_nCr is displayed in Figure 4.12.

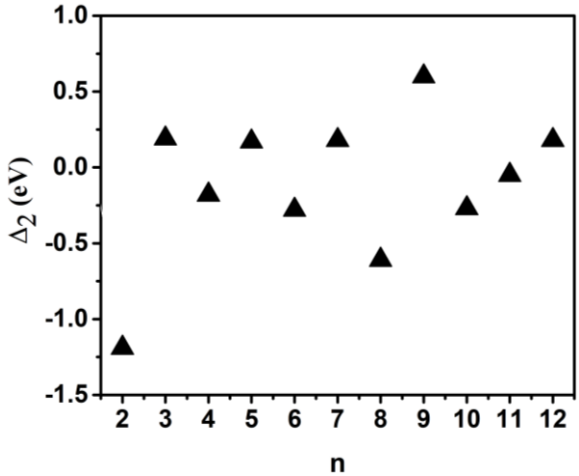

Figure 4.12. The second-order bond energy difference (Δ_2E, eV) of Ag_nCr (n = 2-12) nanoclusters.

The calculation of second-order bond energy difference indicates that the Ag_9Cr nanocluster exhibits higher stability compared to neighboring cluster size. It suggests that Ag_9Cr is relatively more stable than other nearby cluster sizes in the Ag_nCr series.

4.2.2.3. Dissociation energy of Ag_nCr nanoclusters

The dissociation energy (*DE*, eV) of Ag_nCr nanoclusters through the two possible channels is calculated as follows:

$$DE(\text{Ag}) = E(\text{Ag}_{n-1}\text{Cr}) + E(\text{Ag}) - E(\text{M}_n\text{Ag}) \qquad (4.15)$$

$$DE(\text{Cr}) = E(\text{Ag}_n) + E(\text{Cr}) - E(\text{Ag}_n\text{Cr}) \qquad (4.16)$$

The analysis of the calculated dissociation energy of Ag_nCr (n = 2-12) reveals the following findings. For nanoclusters with small size n ≤ 8, the dissociation channel that removes a Cr atom is favored in terms of energy. Conversely, for larger size n = 9-12, the preferred dissociation channel shifts towards the removal of a single Ag atom over a single Cr atom. The Ag_9Cr nanocluster exhibits the highest stability, requiring a minimum energy of 2.58 eV to dissociate a single Ag atom. Notably, this dissociation energy value is even higher than that of the $Ag_{12}Cr$ (2.30 eV).

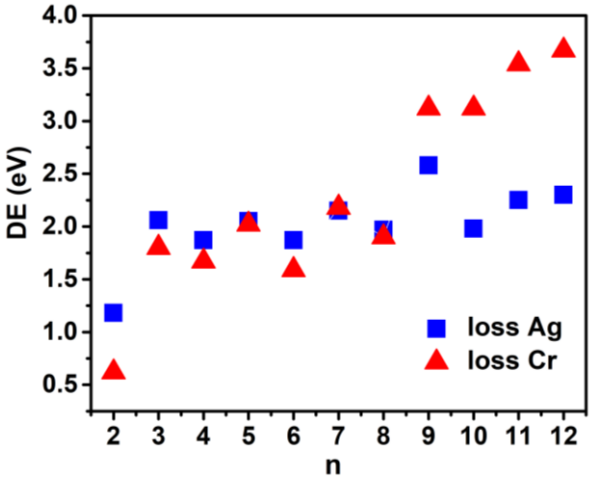

Figure 4.13. The dissociation energy of Ag_nCr (n = 1-12) nanoclusters.

The calculated results of binding energy, second-order energy difference, and dissociation energy demonstrate that Ag_9Cr nanoclusters exhibit the highest stability among the studied Ag_nCr (n = 2-12) nanoclusters. This finding suggests that Ag_9Cr is highly suitable for experimental fabrication and synthesis.

4.2.3. Hydrogen adsorption process on Ag_nCr nanoclusters

4.2.3.1. The geometric structure of $Ag_nCr@H_2$ nanoclusters

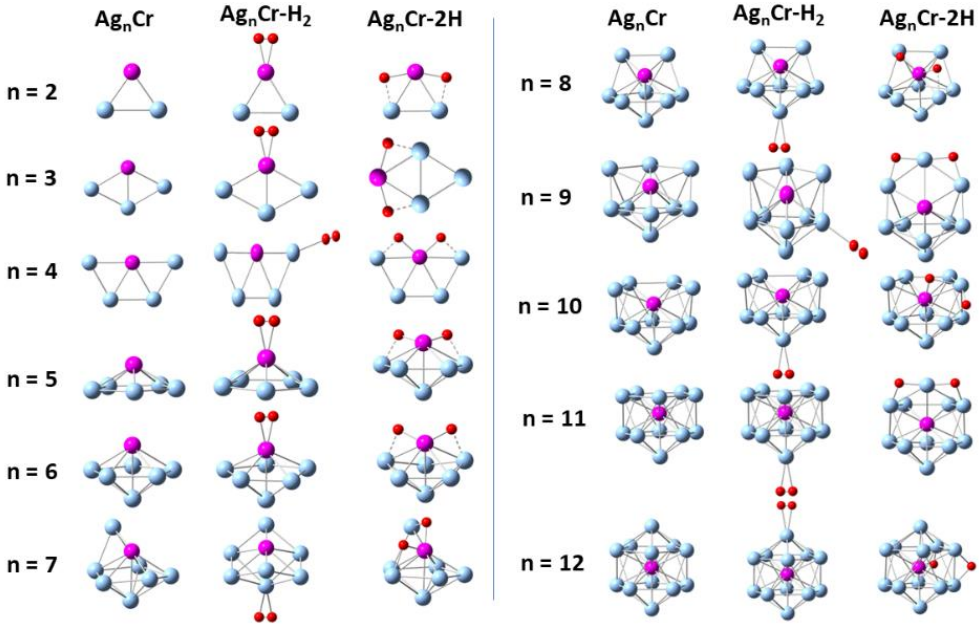

Figure 4.14. The optimized structures of Ag_nCr, $Ag_nCr\text{-}H_2$, and $Ag_nCr\text{-}2H$ (n = 2-12) nanoclusters are represented, with light blue, purple and red colors indicating Ag, Cr, and H atoms, respectively.

The stable geometric structures of Ag_nCr (n = 2-12) nanoclusters adsorbing H_2 were obtained using the BP86 functional combined with the cc-pVTZ-pp, cc-pVTZ, and SDD basis sets for Ag, Cr, and H, respectively. Two forms of adsorption were observed: hydrogen molecular adsorption (Ag_nCr-H_2) and two single hydrogen atoms adsorption (Ag_nCr-2H) for each cluster size. The results are presented in Figure 4.14.

The geometric structure of Ag_nCr nanoclusters remains mostly preserved in both molecular and dissociative adsorption. Our study indicates that the size and composition of the nanoclusters can influence the adsorption of H_2 at different positions, including Ag atom sites, Ag-Ag bridge sites, Ag-Cr bridge sites, or even at the central transition metal atom sites.

4.2.3.2. The stability of $Ag_nCr@H_2$ nanoclusters

The relative stability of $Ag_nCr@H_2$ nanoclusters is determined through the analysis of average binding energy and second-order energy difference.

Average binding energy

The average binding energy of each atom in the Ag_nCr-H_2 and Ag_nCr-2H molecular and dissociative adsorption nanoclusters (n = 2-12) is determined using equations 4.17 and 4.18, respectively.

$$BE(Ag_nCr - H_2) = \frac{1}{n+3}\left[nE_{Ag} + E_{Cr} + 2E_H - E(Ag_nCr - H_2)\right] \quad (4.17)$$

$$BE\ (Ag_nCr - 2H) = \frac{1}{n+3}\left[nE_{Ag} + E_{Cr} + 2E_H - E(Ag_nCr - 2H)\right] \quad (4.18)$$

Where E(Ag_nCr-H_2), E(Ag_nCr-2H), E(Ag), E(Cr), and E(H) represents the energy of Ag_nCr-H_2, Ag_nCr-2H (n = 2-12) nanoclusters, Ag, Cr, and H atoms, respectively.

The calculation of average binding energy reveals that the highest peaks occur at clusters size of n = 3, 6, and 9 for Ag_nCr-H_2 nanoclusters, and n = 3, 9 for Ag_nCr-2H nanoclusters. These results are consistent with the relatively high stability exhibited by Ag_3Cr, Ag_6Cr và Ag_9Cr nanoclusters.

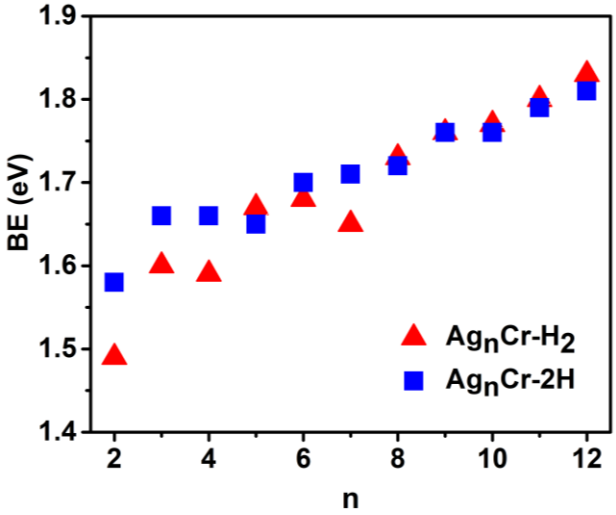

Figure 4.15. The average binding energy (*BE*, eV) of Ag_nCr-H_2 and Ag_nCr-2H (n = 2-12) nanoclusters.

Second-order energy difference

The second-order energy difference is computed by calculating the energy difference between a nanocluster and its neighboring size, as described by equations 4.19 and 4.20.

$$\Delta_2E[Ag_nCr\text{-}H_2] = E[Ag_{n-1}Cr\text{-}H_2] + E[Ag_{n+1}Cr\text{-}H_2] - 2E[Ag_nCr\text{-}H_2] \quad (4.19)$$

$$\Delta_2 E[Ag_nCr\text{-}2H] = E[Ag_{n-1}Cr\text{-}2H] + E[Ag_{n+1}Cr\text{-}2H] - 2E[Ag_nCr\text{-}2H] \quad (4.20)$$

Where E is the total energy of nanoclusters.

The analysis of average binding energy (BE, eV) and dissociation energy reveals that, at sizes n = 3 and 9, both $Ag_nCr\text{-}H_2$ and $Ag_nCr\text{-}2H$ nanoclusters exhibit a significantly higher level of stability compared to their neighboring sizes.

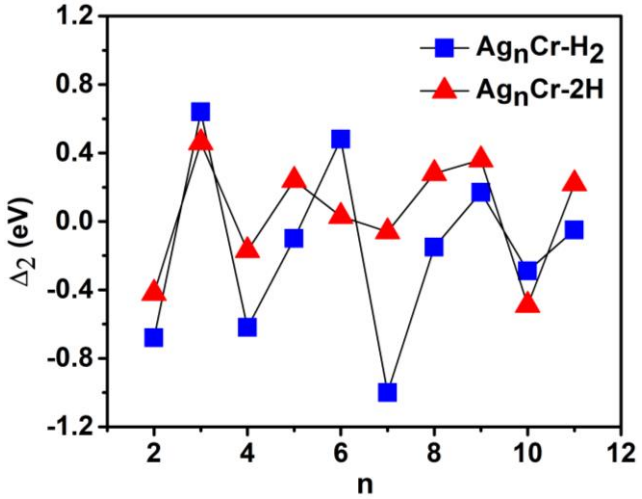

Figure 4.16. The second-order energy difference (Δ_2E, eV) of $Ag_nCr\text{-}H_2$ and $Ag_nCr\text{-}2H$ (n = 2-12) nanoclusters.

4.2.3.3. Kinetic state of Ag_nCr nanocluster during binding with H_2

To investigate the ability of H_2 adsorption on Ag_nCr nanoclusters, the adsorption energy and H-H bond length are calculated for both molecular and atomic adsorption processes as follows and the results are presented in Table 4.6:

$$E_{ads}(Ag_nCr - H_2) = E(Ag_nCr) + E(H_2) - E(Ag_nCr - H_2) \quad (4.9)$$

$$E_{ads}(Ag_nCr - 2H) = E(Ag_nCr) + E(H_2) - E(Ag_nCr - 2H) \quad (4.10)$$

Table 4.6. Adsorption energy E_{ads} (eV) and H-H bond lengths ($d_{H\text{-}H}$, Å) of $Ag_nCr\text{-}H_2$ and Ag_n-Cr-2H (n = 2-12) nanoclusters.

n	E_{ads}/eV		d(H-H)/Å	
	$AgCrH_2$	**AgCr-2H**	**$AgCrH_2$**	**AgCr-2H**
2	0.58	0.80	0.80	3.57
3	0.77	1.13	0.79	3.63
4	0.48	0.96	0.76	2.67
5	0.77	0.63	0.79	2.68
6	0.72	0.86	0.79	2.93
7	0.05	0.65	0.77	2.38
8	0.67	0.56	0.76	2.72
9	0.23	0.20	0.76	3.51
10	0.23	0.06	0.77	3.20
11	0.24	0.15	0.77	3.52
12	0.25	-0.04	0.77	3.97

The H-H bond lengths ($d_{H\text{-}H}$, Å) of $Ag_nCr\text{-}H_2$ nanoclusters at n = 2, 3, 5, and 6 were found to fall within the range of 0.79 to 0.82 Å, compared to the isolated H_2 molecule (0.75 Å). The elongation of the H-H bond length indicates that the H_2 molecule undergoes activation upon adsorption onto the surface of the Ag_nCr alloy nanoclusters. The adsorption energy study reveals that the adsorption of

H_2 molecules occurs for Ag_nCr nanoclusters at n = 5 and 8-12. On the other hand, upon approaching the surface of Ag_nCr nanoclusters (n = 2-4, 6, and 7), H_2 undergoes molecular adsorption and eventually dissociates to form stable bonds with the nanocluster.

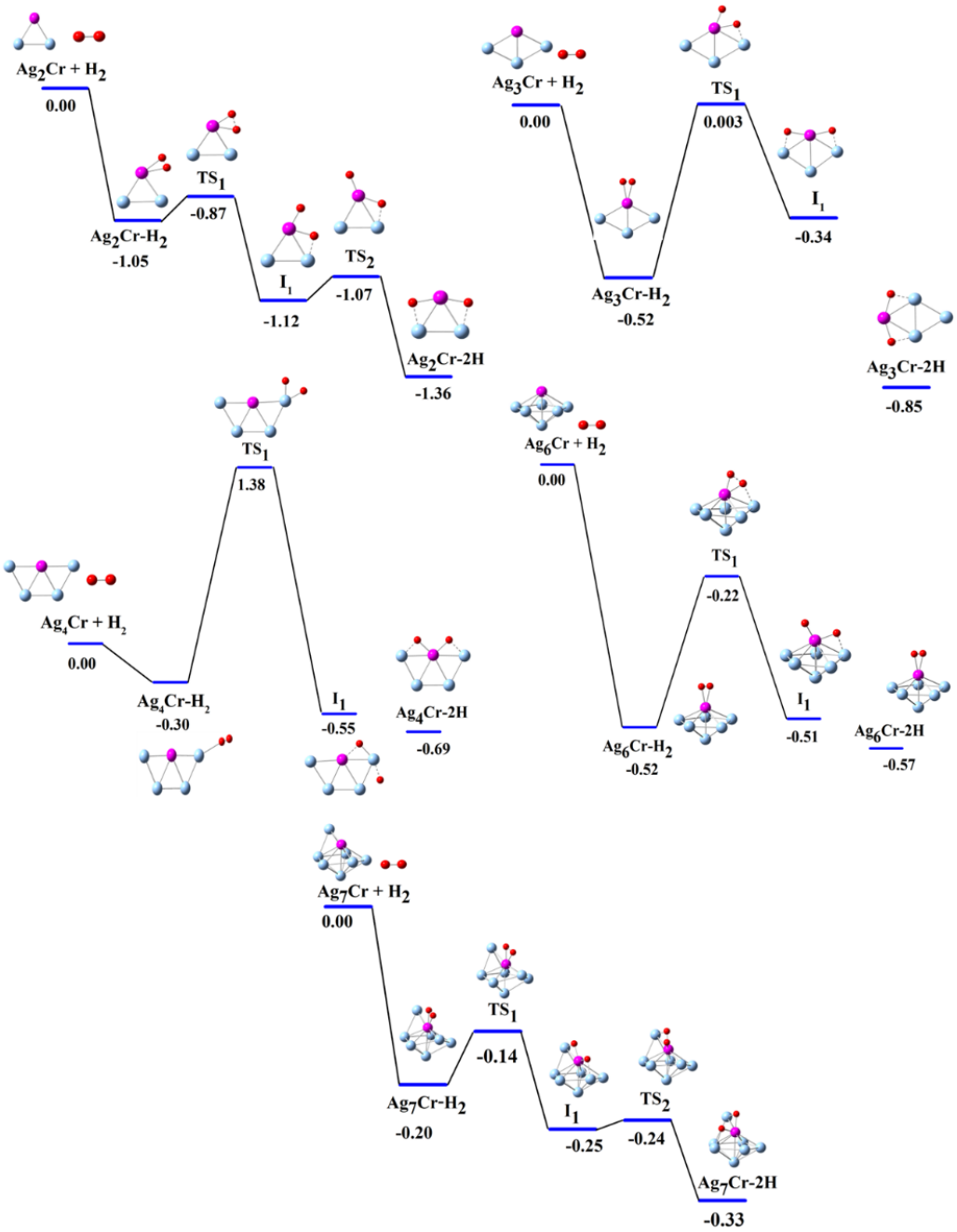

Figure 4.20. The reaction pathways and relative free energies (eV) for molecular adsorption and dissociation of H_2 on Ag_nCr nanoclusters (n = 2-4, 6-7)

To investigate the nature of hydrogen bonding adsorbed on Ag_nCr nanoclusters, we performed calculations of partial density of states (pDOS) and total density of states (DOS) for the adsorbed nanoclusters in both forms of hydrogen adsorption: Ag_nCr-H_2 and Ag_nCr-2H.

The hydrogen adsorption process on Ag_3Cr and Ag_6Cr nanoclusters experiences relatively small energy barriers (0.52 eV and 0.30 eV) for hydrogen dissociation activation. Therefore, Ag_3Cr-2H and Ag_6Cr-2H nanoclusters are regarded as potential superatoms for hydrogen storage.

The mechanism of how the electronic *s-d* interaction influences the stable geometric structure of Ag_nCr nanoclusters and the adsorption of hydrogen on these nanoclusters is presented in Table 4.8.

Table 4.8. The fluence of the electronic *s-d* interaction on the stable geometric structure of Ag_nCr nanoclusters and their interaction with H_2.

n	Electronic structure of Ag_nCr	Electronic structure components of Ag_nCr	Geometric structure Ag_nCr	E_{ads}, eV		Activation energy barrier, eV
				Ag_nCr-H_2	Ag_nCr-2H	
2	$1S^21P^23d^{4\uparrow}$	Cr: contributes 1 electron from 3*d* orbital and 1 electron from 4*s* orbital.	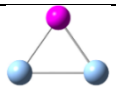	0.58	0.80	0.18
3	$1S^21P^23d^{5\uparrow}$	Cr: contributes 1 electron from 4*s* orbital	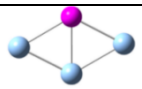	0.77	1.13	0.52
4	$1S^21P^43d^{4\uparrow}$	Cr: contributes 1 electron from 3*d* orbital and 1 electron from 4*s* orbital..	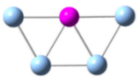	0.48	0.96	1.68
5	$1S^21P^43d^{5\uparrow}$	Cr: contributes 1 electron from 4*s* orbital.	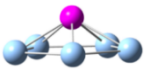	0.77	0.63	-
6	$1S^21P^43d^{5\uparrow}1P^{1\uparrow}$	Cr: contributes 1 electron from 4*s* orbital.	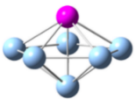	0.72	0.86	0.30
7	$1S^21P^63d^{5\uparrow}$	Cr: contributes 1 electron from 4*s* orbital.	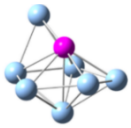	0.05	0.65	0.06
8	$1S^21P^61D^23d^{4\uparrow}$	Cr: contributes 1 electron from 3*d* orbital and 1 electron from 4*s* orbital..	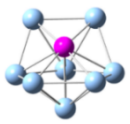	0.67	0.56	-
9	$1S^21P^61D^43d^{3\uparrow}$	Cr: contributes 2 electrons from 3*d* orbital and 1 electron from 4*s* orbital.	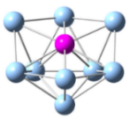	0.23	0.20	-
10	$1S^21P^61D^63d^{2\uparrow}$	Cr: contributes 3 electrons from 3*d* orbital and 1 electron from 4*s* orbital.	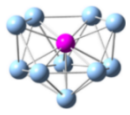	0.23	0.06	-
11	$1S^21P^61D^83d^{1\uparrow}$	Cr: contributes 4 electrons from 3*d* orbital and 1 electron from 4*s* orbital.	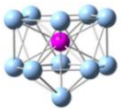	0.24	0.15	-
12	$1S^21P^61D^{10}$	Cr: contributes 5 electrons from 3*d* orbital and 1 electron from 4*s* orbital.	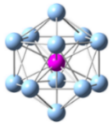	0.25	-0.04	-

4.3. Conclusion of chapter 4

In chapter 4, We has investigated the geometric structure and stability of Au_9M^{2+} and Ag_nCr nanoclusters and also determined the kinetic reaction dynamics of hydrogen on these nanoclusters.

The stable geometric structures of Au_9Sc^{2+} and Au_9Ti^{2+} nanoclusters exhibit a cage-like form. The presence of heavier transition metal impurities (M = V-Ni) in the Au_9M^{2+} clusters tends to maintain a similar tetrahedral structure as that of the Au_{10}^{2+} nanoclusters, resembling the geometric structure of $Au_{19}M$ (M = Cr-Ni) and Au_{20} nanoclusters. The V impurity serves as the starting point for the structural transition from the cage-like form to the tetrahedral structure. Ag_nCr nanoclusters tend to form 2D structures at small sizes (n = 2-5). The transition from 2D to 3D geometric structures occurs at n = 6.

The investigation results on the interaction between Au_9M^{2+} nanoclusters and hydrogen reveal that the adsorption of H_2 molecules is favorable for Au_9M^{2+} clusters (M = Sc, Mn, and Fe), but the H_2 dissociation process requires a relatively high energy barrier (0.70 eV, 0.94 eV, and 1.31 eV) to activate the hydrogen dissociation process. In contrast, the hydrogen adsorption process on Au_9Ti^{2+} nanoclusters encounters a small energy barrier (0.59 eV) to activate hydrogen dissociation, making Au_9Ti^{2+} clusters potential superatomic hydrogen storage units. For Ag_nCr nanoclusters, at sizes n = 2, 3, 4, 6, and 7, the adsorption of two H atoms is energetically favored over the adsorption of H_2 molecules. Particularly, the hydrogen adsorption process on Ag_3Cr and Ag_6Cr nanoclusters has a relatively small energy barrier (0.52 eV and 0.30 eV) to activate hydrogen dissociation, thus making Ag_3Cr-2H and Ag_6Cr-2H clusters potential superatomic hydrogen storage units.

CONCLUSION

In this thesis, the density functional theory method employing the BP86 functional in combination with appropriate basis sets was utilized to investigate alloy nanoclusters including Au_9M^{2+} (M = Sc-Ni) and Ag_nCr (n = 2-12). The thesis achieved several results, including:

1. The thesis successfully identified the *s-d* interaction of noble metal (Au, Ag) nanoclusters with 3*d* transition metal impurities and elucidated the role of this interaction in the formation of geometric structures and stability of the nanoclusters.

2. The research extensively investigated the indirect influence of *s-d* interaction on the adsorption and dissociation of hydrogen on Au_9M^{2+} and Ag_nCr nanoclusters through the analysis of geometric structures, electronic structures, coordination numbers, and electronegativity.

3. Au_9Ti^{2+}, Ag_3Cr, and Ag_6Cr are stable nanoclusters that have the ability to readily adsorption and dissociate H_2 to form hydrides even at room temperature conditions.

NEW CONTRIBUTIONS OF THE THESIS

The thesis successfully determined the stable geometric structures, corresponding electronic structures, and reaction kinetics with H2 of the alloy nanoclusters Au_9M^{2+} (M = Sc-Ni) and Ag_nCr (n = 2-12). The thesis clarified the influence of the interaction between delocalized electrons and localized electrons on the structural transformations, electronic structures, and reactions with H2 of the alloy nanoclusters Au_9M^{2+} (M = Sc-Ni) and Ag_nCr (n = 1-12).

RECOMMENDATIONS FOR FURTHER RESEARCH

The study of the physical interaction between delocalized and localized electrons in noble metal nanoclusters containing transition metals plays a crucial role in investigating potential materials for catalysis, especially hydrogen adsorption. The research results on hydrogen adsorption in Au_9M^{2+} (M = Sc-Ni) and Ag_nCr (n = 2-12) alloy nanoclusters using initial quantum calculations demonstrate an effective approach to elucidate the hydrogen adsorption mechanism on the surfaces of these alloy nanoclusters. This knowledge serves as a foundation to assist in the efficient design and fabrication of hydrogen storage materials with improved orientation and cost-effectiveness.

Furthermore, the influence of the interaction between delocalized and localized electrons on the magnetic properties of alloy nanoclusters is of great interest for advanced materials applications. Although the electron structure and spin moment of Au_9M^{2+} (M = Sc-Ni) and Ag_nCr (n = 2-12) nanoclusters have been studied in the thesis, the magnetic properties depend on the spin-orbit interaction within the nanoclusters. Therefore, computational studies on spin-orbit interactions will enhance the understanding of the magnetic properties of these nanoclusters as well as other potential superatomic systems in the future.

LIST OF THE PUBLICATIONS RELATED TO THE DISSERTATION

List of publications in the SCIE category:

1. Ngo Thi Lan, Nguyen Thi Mai, Duong Duc La, Son Tung Ngo, Nguyen Minh Tam, Nguyen Van Dang, Nguyen Thanh Tung, "*Exploring hydrogen adsorption on nanocluster systems: Insights from DFT calculations of Au_9M^{2+} (M = Sc-Ni)*", Chemical Physics Letters, (2023), 831, 140838.

2. Ngo Thi Lan, Nguyen Thi Mai, Ngo Tuan Cuong, Phung Thi Hong Van, Duong Duc La, Nguyen Minh Tam, Son Tung Ngo, and Nguyen Thanh Tung, "*Density Functional Study of Size-Dependent Hydrogen Adsorption on Ag_nCr (n = 1−12) Clusters*", ACS Omega 2022, 7, 42, 37379–37387.

3. Ngo Thi Lan, Nguyen Thi Mai, Duong Duc La, Nguyen Minh Tam , Son Tung Ngo, Ngo Tuan Cuong, Nguyen Van Dang, Thu Thi Phung, Nguyen Thanh Tung, "*DFT investigation of Au_9M^{2+} nanoclusters (M = Sc-Ni): The magnetic superatomic behavior of Au_9Cr^{2+}*", Chemical Physics Letters, 2022, 793, 139451.

List of publications in the national journal and conference proceedings

4. Ngo Thi Lan, Nguyen Thi Mai, Nguyen Van Dang and Nguyen Thanh Tung, "*DFT investigation of pyramidal Au_9M^{2+} and $Au_{19}M$ (M = Sc-Ni): Similarities and differences of structural evolution, electronic and magnetic properties*", Commuications in Physics, 2023, 33, 1, 63-72.

5. Nguyen Thi Mai, **Ngo Thi Lan**, Nguyen Thanh Tung, "*Geometries, stability and dissociation behavior of Ag_nCo clusters (n = 1-12): A theoretical investigation*", Journal of Military Science and Technology, 2023, 86, 103-109.

6. Ngo Thi Lan, Nguyen Thi Mai, Bui Son Tung, Nguyen Van Dang, and Nguyen Thanh Tung, "*Structures, stabilities and infrared spectra of Ag_nCr clusters (n=2-12) by density functional theory calculation*", Journal of Military Science and Technology, 2022, 77, 02.

7. Ngo Thi Lan, Nguyen Thi Mai, Ngo Tuan Cuong, Nguyen Thanh Tung, "*Co-existence of localized magnetic moment and delocalized electronic shell in sub-nanometer Kondo-like systems*", Journal of Military Science and Technology, 2020, 68, 8.

8. Nguyen Thi Mai, **Ngo Thi Lan**, Phung Thi Thu, Nguyen Van Dang**,** and Nguyen Thanh Tung, "*A theoretical investigation on $CrCu_n$ (n = 1÷8) clusters: geometry, stability, and magnetic properties*", The 10th International Workshop on Advanced Materials Science and Nanotechnology (IWAMSN 2021), November 4-6th, 2021, Hanoi, Vietnam.